Supporting Information

General Synthesis of MFe_2O_4/Carbon (M=Zn, Mn, Co, Ni) Spindles from Mixed Metal Organic Frameworks as High Performance Anodes for Lithium Ion Batteries

Zhong-Jie Jiang,[*,a] Si Cheng,[a] Haibo Rong,[a] Zhongqing Jiang[b] and Jianlin Huang [a]

[a] Guangzhou Key Laboratory for Surface Chemistry of Energy Materials, New Energy Research Institute, College of Environment and Energy, South China University of Technology, Guangzhou 510006, Guangdong, China. E-mail: zhongjiejiang1978@hotmail.com; esjiang@scut.edu.cn; Tel: +86-020-39381202.

[b] School of Materials and Chemical Engineering, Ningbo University of Technology, Ningbo 315211, Zhejiang, China.

Contents

1. TGA curve of the $ZnFe_2O_4$/C spindles.

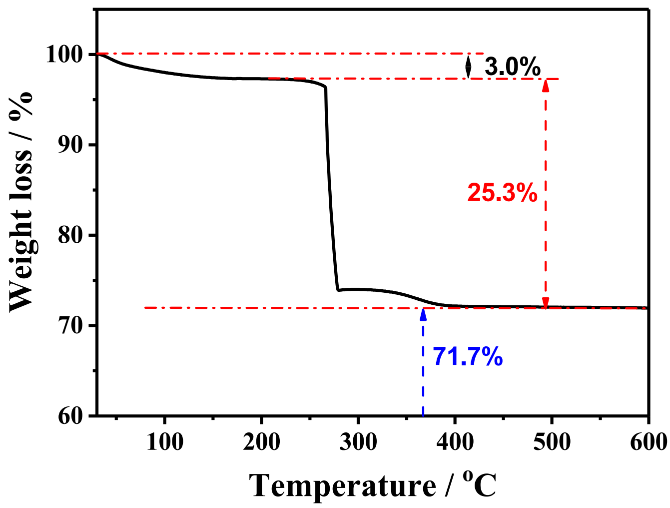

Figure S1. TGA curve of the $ZnFe_2O_4$/C spindles.

The weight loss below 150°C could be ascribed to the removal of the physically adsorbed water. The weight loss at 240-410°C would be attributed to the removal of the carbon framework. Based on the TGA, it could be inferred that the $ZnFe_2O_4$/C spindles contain 3.0 wt.% of the physically adsorbed water, 25.3wt.% of carbon, and 71.7 wt. % of $ZnFe_2O_4$.

2. Comparison of the XRD pattern of the $ZnFe_2O_4$/C spindles with those of the standard $ZnFe_2O_4$, Fe_3O_4 and ZnO.

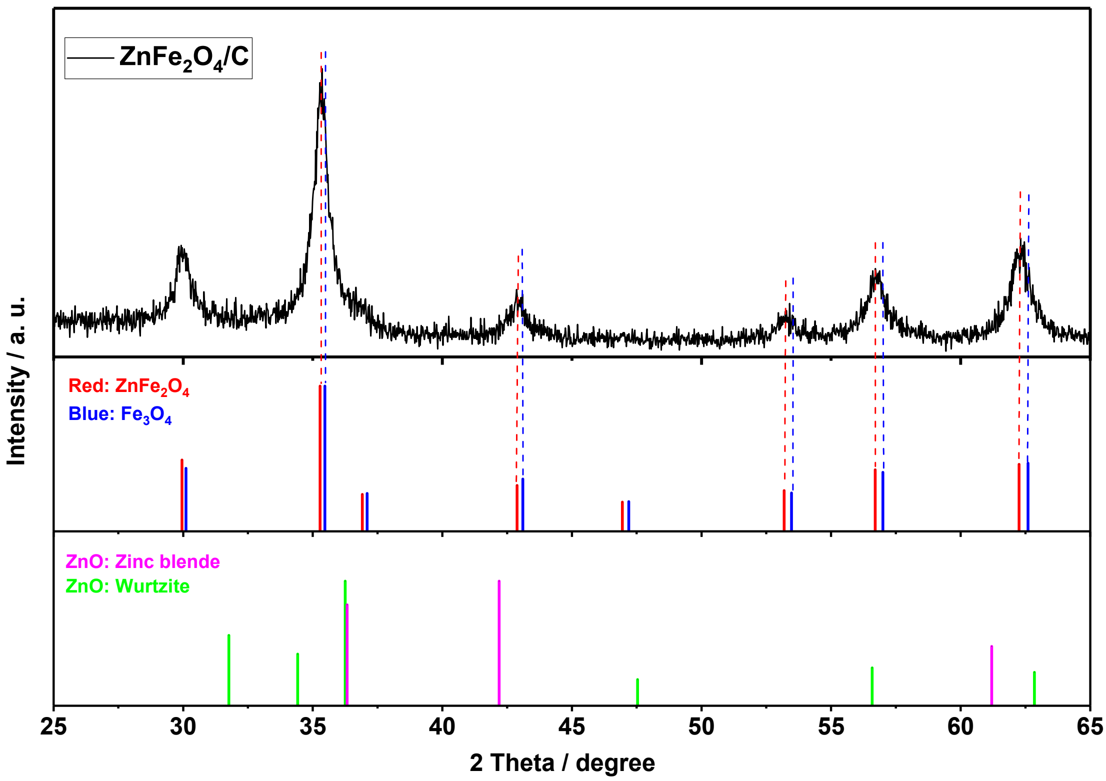

Figure S2. Comparison of the XRD pattern of the $ZnFe_2O_4$/C spindles with those of the standard $ZnFe_2O_4$, Fe_3O_4 and ZnO.

The XRD pattern clearly shows that the diffraction peaks of the $ZnFe_2O_4$/spindles better match with those of the the cubic spinel $ZnFe_2O_4$ (JCPDS card no. 89-1010). Although the spinel structured Fe_3O_4 has a diffraction pattern similar to $ZnFe_2O_4$, its diffraction peaks do not match well with the $ZnFe_2O_4$/spindles. Additionally, the diffraction pattern also indicates the absence of the ZnO phase in the $ZnFe_2O_4$/C spindles. As shown in the Figure S2, there are no diffraction peaks assignable to Wurtzite and/or Zinc blende structured ZnO in the XRD pattern of the $ZnFe_2O_4$/spindles. This, along with the uniform distribution of Zn, Fe and O in the $ZnFe_2O_4$/C spindles, as demonstrated in the elemental mapping image shown in Figure 2a, strongly suggest that Zn and Fe exist in the form of $ZnFe_2O_4$.

3. Elemental mapping of Zn, Fe, O, and C in the $ZnFe_2O_4$/C spindles.

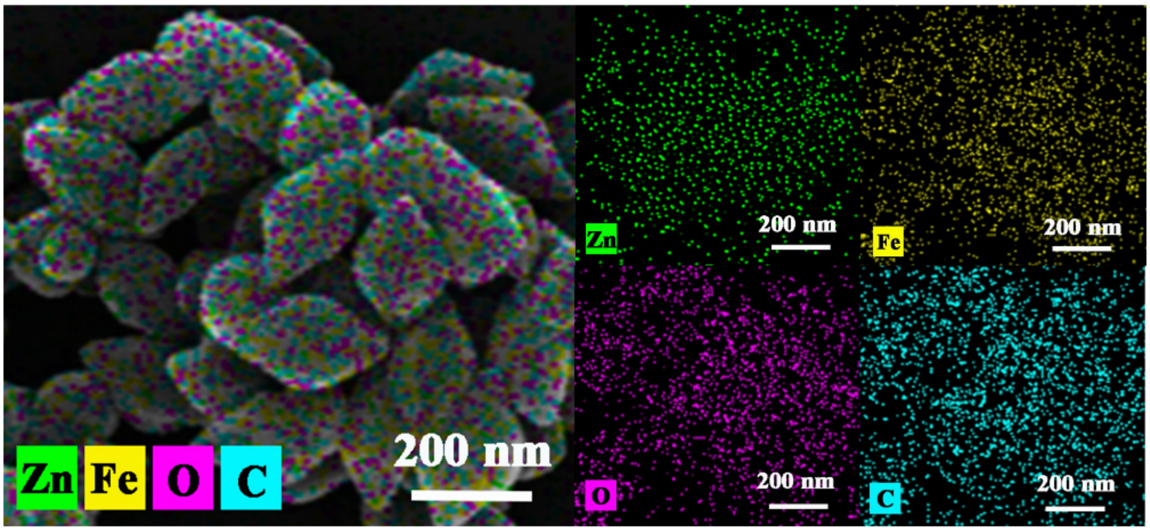

Figure S3. Elemental mapping of Zn, Fe, O, and C in the $ZnFe_2O_4$/C spindles.

4. XPS survey spectra of the $ZnFe_2O_4$/C, $MnFe_2O_4$/C, $CoFe_2O_4$/C, and $NiFe_2O_4$/C spindles.

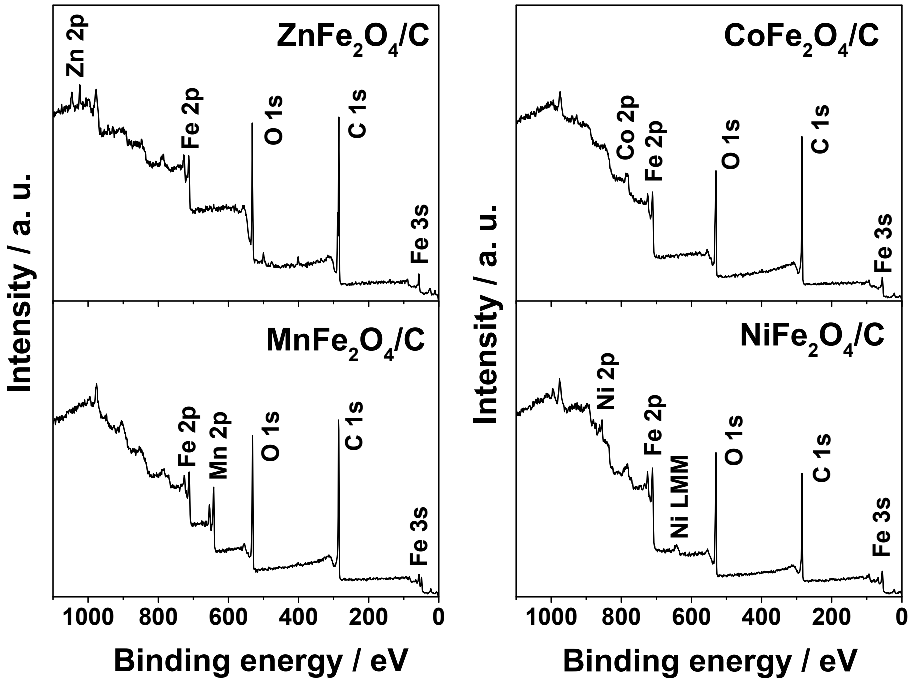

Figure S4. XPS survey spectra of the $ZnFe_2O_4$/C, $MnFe_2O_4$/C, $CoFe_2O_4$/C, and $NiFe_2O_4$/C spindles.

5. XRD diffraction patterns of the $MnFe_2O_4$/C, $CoFe_2O_4$/C, and $NiFe_2O_4$/C spindles.

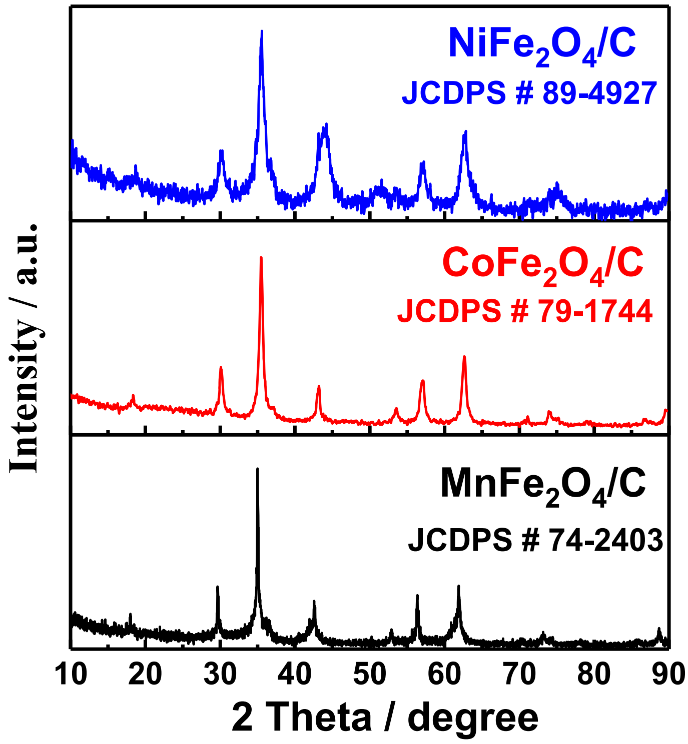

Figure S5. XRD diffraction patterns of the $MnFe_2O_4$/C, $CoFe_2O_4$/C, and $NiFe_2O_4$/C spindles.

6. XPS spectra of Mn 2p, Co 2p, Ni 2p, Fe 2p, O 1s, and C 1s for the $MnFe_2O_4$/C, $CoFe_2O_4$/C, and $NiFe_2O_4$/C spindles.

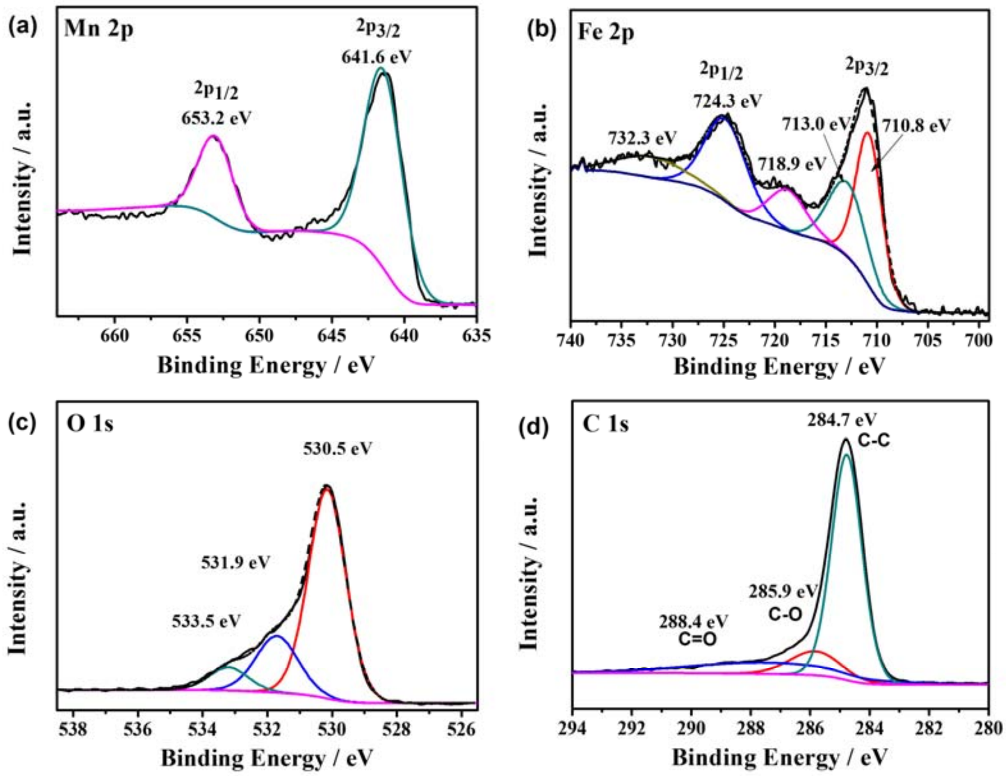

Figure S6. XPS spectra of (a) Mn 2p, (b) Fe 2p, (c) O 1s, and (d) C 1s for the $MnFe_2O_4$/C spindles.

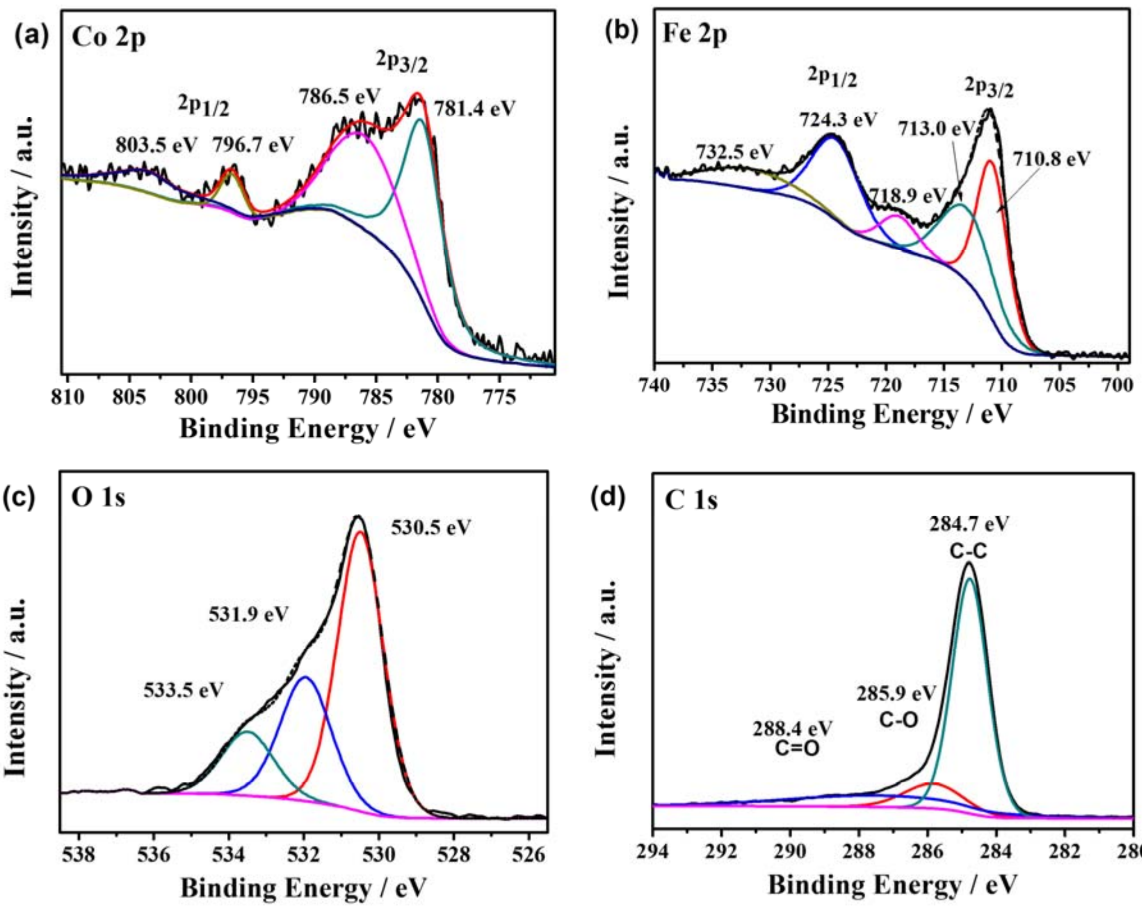

Figure S7. XPS spectra of (a) Co 2p, (b) Fe 2p, (c) O 1s, and (d) C 1s for the $CoFe_2O_4$/C spindles.

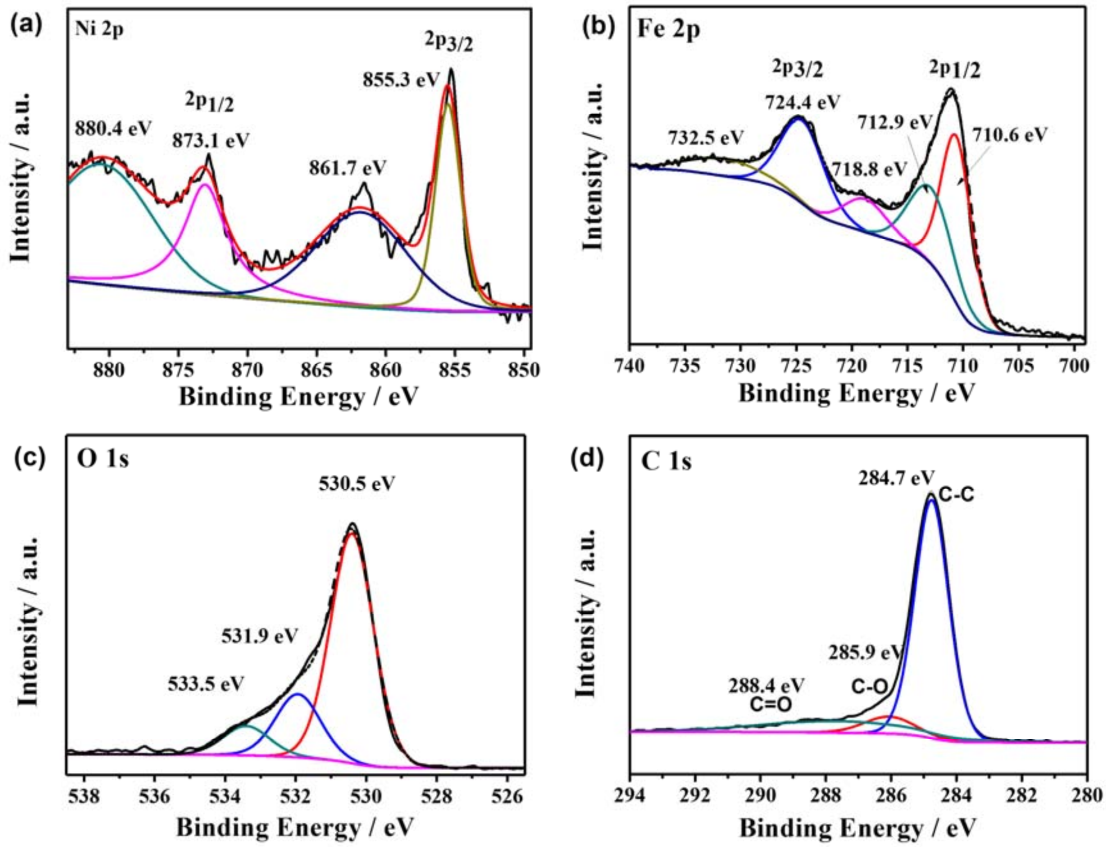

Figure S8. XPS spectra of (a) Ni 2p, (b) Fe 2p, (c) O 1s, and (d) C 1s for the $NiFe_2O_4$/C spindles.

7. N_2 adsorption/desorption isotherms of the MFe_2O_4/C ((M= Zn, Mn, Co, Ni)) spindles.

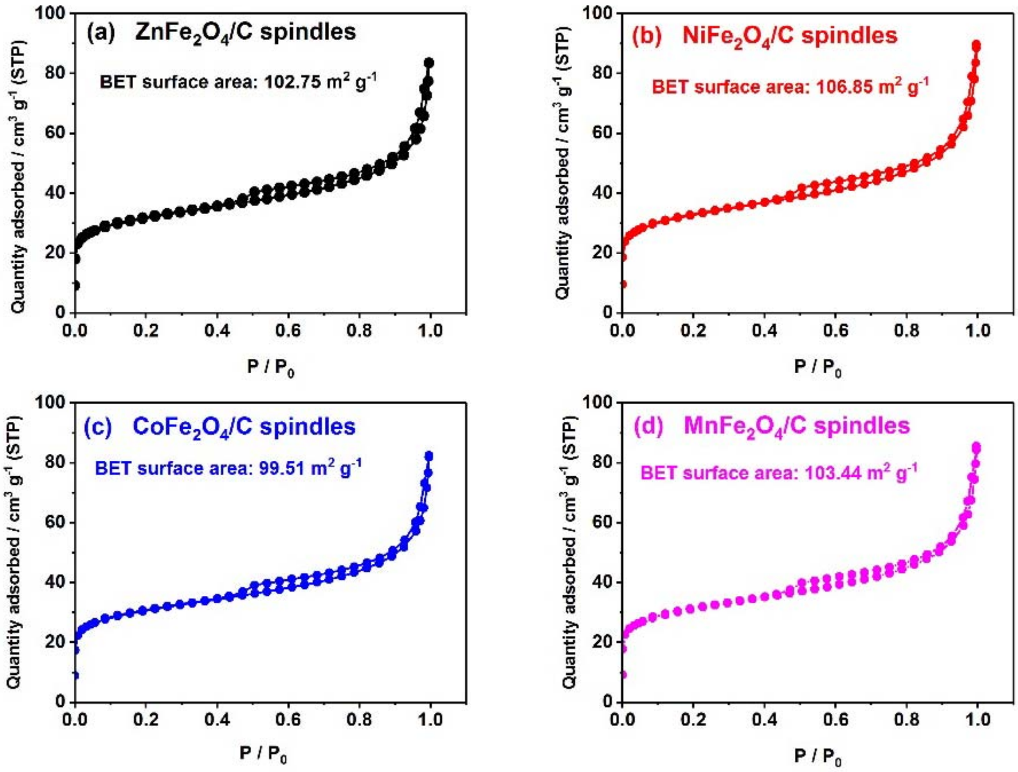

Figure S9. N_2 adsorption/desorption isotherms of the MFe_2O_4/C ((M= Zn, Mn, Co, Ni)) spindles. The specific surface areas of the samples were calculated using the Brunauer−Emmett−Teller (BET) method.

8. Reaction Schemes for the MFe_2O_4/C(M=Zn, Mn, Co, Ni) spindles as the anode for LIBs.

(1) $ZnFe_2O_4 + xLi^+ + xe^- \rightarrow Li_xZnFe_2O_4$

(2) $Li_xZnFe_2O_4 + (8-x)Li^+ + (8-x)e^- \rightarrow Zn^0 + 4Li_2O + 2Fe^0$

(3) $Zn^0 + Li^+ + e^- \leftrightarrow LiZn$

(4) $Zn^0 + Li_2O \leftrightarrow ZnO + 2Li^+ + 2e^-$

(5) $2Fe^0 + 3Li_2O \leftrightarrow Fe_2O_3 + 6Li^+ + 6e^-$

Scheme S1. Reactions associated with the discharge/charge processes of the $ZnFe_2O_4$/C spindles[1]

(1) $MFe_2O_4 + xLi^+ + xe^- \rightarrow Li_xMFe_2O_4$

(2) $Li_xMFe_2O_4 + (8-x)Li^+ + (8-x)e^- \rightarrow M^0 + 4Li_2O + 2Fe^0$

(3) $M^0 + Li_2O \leftrightarrow MO + 2Li^+ + 2e^-$

(4) $2Fe^0 + 3Li_2O \leftrightarrow Fe_2O_3 + 6Li^+ + 6e^-$

Scheme S2. Reactions associated with the discharge/charge processes of the MFe_2O_4/C (M= Mn, Co, Ni) spindles[2]

9. Charge/discharge capacities of the carbon spindles at the current rates of 0.4 and 1.6 C.

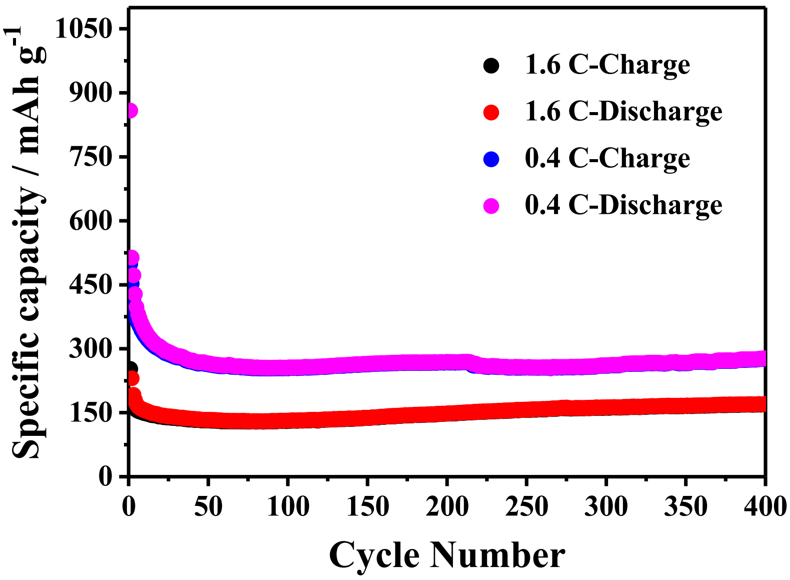

Figure S10. Charge/discharge capacities of the carbon spindles at the current rates of 0.4 and 1.6 C.

10. Comparison of the stable reversible capacity of the $ZnFe_2O_4$/C spindles with other $ZnFe_2O_4$ based anodes and Comparison of the stable reversible capacity of the MFe_2O_4/C(M=Mn, Co, Ni) spindles with other MFe_2O_4 (M=Mn, Co, Ni) based anodes.

Table S1. Comparison of the stable reversible capacity of the $ZnFe_2O_4$/C spindles with other $ZnFe_2O_4$ based anodes.

Materials	Mass loading of each electrode/ mg cm^{-2}	Current rate / mA g^{-1}	Capacity / mA h g^{-1}	Number of cycles	Ref.
$ZnFe_2O_4$/graphene ($ZnFe_2O_4$/G)	-	200	600	5	3
Hierarchical Porous Acetylene Black/ $ZnFe_2O_4$@Carbon (AB/$ZnFe_2O_4$@Carbon)	1.2~1.7	100	803	150	4
Porous hierarchical Nitrogen-doped carbon $ZnFe_2O_4$ ($ZnFe_2O_4$/NC)	1.6	100	809	50	5
$ZnFe_2O_4$ nanooctahedrons ($ZnFe_2O_4$ Oh)	-	60	910	80	6
Core-shell ZnO/$ZnFe_2O_4$@C mesoporous nanospheres (ZnO/$ZnFe_2O_4$@C)	-	500	893	60	7
Hierarchical Mesoporous Bi-Component-Active ZnO/$ZnFe_2O_4$ Sub-Microcubes (Bi-ZnO/$ZnFe_2O_4$)	0.9 mg per Cu foil	200	950	An average of 10 discharge capacities	8
3D mesoporous $ZnFe_2O_4$-graphene composites (3D $ZnFe_2O_4$/G)	-	500	970	200	9
Hierarchical Shuttle-Shaped Mesoporous $ZnFe_2O_4$ Microrods ($ZnFe_2O_4$ MR)	~1.4 mg per anode	100	896	50	10
$ZnFe_2O_4$-C nanocomposite ($ZnFe_2O_4$/C)	1.5~1.7	71	681	100	11
$ZnFe_2O_4$-nanocrystal-assembled microcages ($ZnFe_2O_4$ cages)	-	100	840	100	12
ultrafine $ZnFe_2O_4$ nanocrystals anchored on graphene ($ZnFe_2O_4$ nc/G)	-	50	822	36	13
$ZnFe_2O_4$@C/graphene		232	712.5	50	14

nanocomposites ($ZnFe_2O_4$@C/G)					
Mesoporous $ZnFe_2O_4$ nanorods ($ZnFe_2O_4$ NR)	0.7	100	983	50	[15]
$ZnFe_2O_4$ Cubes	-	60	367	50	[16]
$ZnFe_2O_4$/C spindles	1.0	200	950	70	This work

Table S2. Comparison of the stable reversible capacity of the MFe_2O_4/C(M=Mn, Co, Ni) spindles with other MFe_2O_4 (M=Mn, Co, Ni) based anodes.

Materials	Mass loading of each electrode/ mg cm^{-2}	Current rate / mA g^{-1}	Capacity / mA h g^{-1}	Number of cycles	Ref.
Mesoporous $MnFe_2O_4$ microspheres	-	185.6	712	50	[17]
Core–Shell $NiFe_2O_4$@TiO_2 Nanorods	-	100	756	60	[18]
$MnFe_2O_4$/graphene	~2 mg per anode	400	706	100	[19]
$MnFe_2O_4$ nanoparticles dispersed on graphene	-	200	904	40	[20]
$MnFe_2O_4$/graphene composites	-	200	684	80	[21]
Carbon-coated $MnFe_2O_4$ nanoparticle hollow microspheres	1.8	200	1024	60	[22]
Hierarchical $NiFe_2O_4$/Fe_2O_3 nanotubes	1.0~1.2 mg per anode	100	936.9	100	[23]
$NiFe_2O_4$/C composite	-	200	600	50	[24]
Electrospun $NiFe_2O_4$@C fibers	1.0~1.5	100	497	100	[25]
Ultrathin NiO/$NiFe_2O_4$ Nanoplates	2.5	100	700	30	[26]
Co_3O_4/$CoFe_2O_4$ Nanocomposite	-	64	756.5	25	[27]
$CoFe_2O_4$/carbon nanotube aerogels	~0.60	100	1033	60	[28]
$CoFe_2O_4$/C composite fiber	-	100	710	40	[29]
$CoFe_2O_4$ quantum dots/N-doped graphene composite	1.0~1.1 mg per anode	100	838	50	[30]
C@$CoFe_2O_4$ fiber-in-	0.7~1.0	200	740	200	[31]

tube mesoporous nanostructure	mg per anode				
$MnFe_2O_4$/C spindles	1.0	200	879	80	This work
$CoFe_2O_4$/C spindles	1.0	200	787	80	This work
$NiFe_2O_4$/C spindles	1.0	200	962	80	This work

References

1. L. Qu, X. Hou, J. Mao, Q. Ru, S. Hu, X. Liu and K.-h. Lam, *RSC Adv.*, 2016, 6, 96743-96751.
2. H. Tang, P. Gao, A. Xing, S. Tian and Z. Bao, *RSC Adv.*, 2014, 4, 28421-28425.
3. W. T. Song, J. Xie, S. Y. Liu, G. S. Cao, T. J. Zhu and X. B. Zhao, *New J. Chem.*, 2012, 36, 2236–2241.
4. J. Caia, H. Wu, Y. Zhu, P. K. Shen and K. Zhang, *Electrochim. Acta*, 2016, 187, 584–592.
5. H. Y. Yue, Q. X. Wang, Z. P. Shi, C. Ma, Y. M. Ding, N. N. Huo, J. Zhang and S. T. Yang, *Electrochim. Acta* 2015, 180, 622–628.
6. Z. Xing, Z. C. Ju, J. Yang, H. Y. Xu and Y. T. Qian, *Nano Res.*, 2012, 5, 477–485.
7. C. Z. Yuan, H. Cao, S. Q. Zhu, H. Hua and L. R. Hou, *J. Mater. Chem. A*, 2015, 3, 20389–20398.
8. L. Hou, L. Lian, L. Zhang, G. Pang, C. Yuan and X. Zhang, *Adv. Funct. Mater.*, 2015 14, 238–246.
9. Y. Dong, Y. Xia, Y.-S. Chui, C. Cao and J. A. Zapien, *J. Power Sources*, 2015, 275, 769-776.
10. H. L, H. Hua, L. Lian, H. Cao, S. Zhu and C. Yuan, *Chem. Eur. J.*, 2015, 21, 13012 – 13019.
11. R. M. Thankachan, M. M. Rahman, I. Sultana, A. M. Glushenkov, S. Thomas, N. Kalarikkal and Y. Chen, *J. Power Sources*, 2015, 282, 462–470.
12. C. Wang, Y. Li, Y. Ruan, J. Jiang and Q.-H. Wu, *Mater. Today Energy*, 2017, 3, 1-8.
13. J. Xie, W. Song, G. Cao, T. Zhu, X. Zhao and S. Zhang, *RSC Adv.*, 2014, 4, 7703–7709.
14. L. Lin and Q. Pan, *J. Mater. Chem. A*, 2015, 3, 1724–1729.
15. X.-B. Zhong, Z.-Z. Yang, H.-Y. Wang, L. Lu, B. Jin, M. Zha and Q.-C. Jiang, *J. Power Sources*, 2016, 306, 718-723.
16. X.-B. Zhong, B. Jin, Z.-Z. Yang, C. Wang and H.-Y. Wang, *RSC Adv.*, 2014, 4, 55173-55178.

17. Z.Zhang, Y. Wang, Q.Tan, Z. Zhong and F. Su, *J. Colloid Interface Sci.*, 2013, 398, 185–192.
18. G. Huang, F.Zhang, X. Du, J. Wang, D. Yin and L. Wang, *Chem. Eur. J.*, 2014, 20, 11214 – 11219.
19. S. Liu, J. Xie, Q. Su, G. Du, S. Zhang, G. Cao, T. Zhu and X. Zhao, *Nano Energy*, 2014, 8, 84–94.
20. Z.Yang, Y.Huang, D. Ji, G. Xiong, H. Luo and Y. Wan, *Ceramics Inter.*, 2017, 43, 10905–10912.
21. S. Li, B. Wang, B. Li, J. Liu, M. Yu and X. Wu, *Mater. Res. Bull.*, 2015, 61, 369–374.
22. Y. Yan, G. Guo, T. Li, D. Han, J. Zheng, J. Hu, D. Yang and A. Dong, *Electrochim. Acta*, 2017, 246, 43–50.
23. G.Huang, F. Zhang, L. Zhang, X. Du, J. Wang and L. Wang, *J. Mater. Chem. A*, 2014, 2, 8048-8053
24. Y. Ding, Y. Yang and H. Shao, *J. Power Sources*, 2013, 244, 610-613.
25. T. Dong, G. Wang and P. Yang, *Diamond Related Mater.*, 2017, 73 210–217.
26. D. Du, W. Yue, X. Fan, K.Tang and X. Yang, *Electrochim. Acta*, 2016, 194, 17–25.
27. A. K. Rai, J. Gim, T. V. Thi, D. Ahn, S. J. Cho and J. Kim, *J. Phys. Chem. C*, 2014, 118 11234–11243.
28. X. Sun, X. Zhu, X. Yang, J. Sun, Y. Xia and D. Yang, *Green Energy Environ.*, 2017, 2, 160-167.
29. L. Wu, Q. Xiao, Z. Li, G. Lei, P. Zhang and L. Wang, *Solid State Ionics*, 2012, 215, 24–28.
30. L. Yao, H. Deng, Q.-A. Huang, Q. Su, X. Du and G. Du, *J. Alloys Compd.*, 2017, 693, 929-935.
31. J. Wang, G. Yang, L. Wang, W. Yan and W. Wei, *J. Alloys Compd.*, 2017, 693, 110-117.